

An Experimental Investigation of Turbulent Boundary Layer Flow over Surface-Mounted Circular Cavities

J. Dybenko, E. Savory

*Department of Mechanical and Materials Engineering, University of Western Ontario, London, Ontario,
jdybenko@uwo.ca, esavory@eng.uwo.ca*

More stringent targets on fuel efficiency for commercial aircraft will require more attention to be paid to drag and noise reduction techniques related to airframe design in the future. One source of drag that could be lessened is that due to the presence of cavities on the surface of the aircraft such as rivet depressions and landing gear wheel wells. In order to gain a greater understanding of the causes of the drag related to such cavities, turbulent flow over circular cavities has been experimentally investigated in a subsonic wind tunnel. Velocity measurements acquired in the cavity wake using hot-wire anemometry and surface pressure measurements collected in the cavity surfaces using pressure transducers and microphones have revealed a link between flow in the cavity and that in its wake. Oscillations in the pressure and velocity time series for $h/D = 0.47$ demonstrated a consistent peak at a frequency expected for the cavity feedback resonance mechanism. Since this peak was not observed at any other depth configuration, it is suggested that cavity feedback resonance may be a cause for the high level of flow asymmetry and cavity drag observed for $h/D = 0.47$. Experiments also allowed the development of a reliable method for switching the sense of asymmetric flow about the stream-wise axis for $h/D = 0.47$. Good agreement was noted between the present results and those from previous investigations.

1. INTRODUCTION

Investigations of the flows over surface-mounted cavities have been quite common due to their fundamental nature. However, most of these investigations have focused on cavities of rectangular planform. Only a few investigators have studied the flow over cavities of circular planform, the focus of the current investigation. Since most studies of this nature have dealt with rectangular cavities, most of the conceptual developments made in this area have been made while studying flow over cavities with that planform.

Rossiter simplified the understanding of cavity-related oscillations by dividing them into three categories: fluid-elastic, fluid-resonant and fluid-dynamic oscillations [1]. Fluid-elastic oscillations occur when a cavity surface itself is forced into oscillation, fluid-resonant oscillations are caused when a self-sustaining oscillation in the flow has a wavelength of the same order as one of the cavity dimensions, and fluid-dynamic oscillations relate to the cavity feedback resonance mechanism defined below.

Rossiter also made another critical conceptual contribution to the study of oscillations resulting from cavity flows with his proposal of the fluid-dynamic mechanism for production of oscillations [1] which has since been confirmed by experiment [2, for example]. This phenomenon is often referred to as cavity feedback resonance and is illustrated in Figure 1. A vortex is shed from the upstream cavity lip (1) and is then convected downstream (2) towards the downstream lip where it impinges causing the generation of an acoustic pressure pulse (3) that radiates upstream (4) and disturbs the shear layer at the upstream cavity lip causing another vortex to be shed (5).

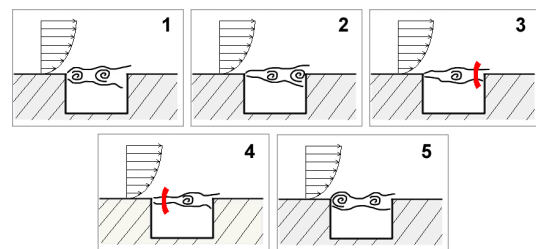


Figure 1: Step-wise illustration of the cavity feedback resonance mechanism.

Due to the self-sustaining nature of this feedback mechanism, acoustic pulses are generated periodically and a narrow-band acoustic tone results. Rossiter also developed an empirical formula to predict the frequency of this tone:

$$f = \frac{U_0(m - \gamma)}{l(M + 1/\kappa)} \quad (1)$$

where f is the predicted frequency of oscillation..

It has been shown that this phenomenon also drastically increases the drag due to the cavity presence, up to 250%, as compared to a cavity under similar conditions not undergoing this type of resonance [3].

Fluid-resonant oscillations are often observed in the flow over circular cavities, a phenomenon somewhat related to the tone heard when blowing across the mouth of a bottle. Oscillations driven by this fluid-resonant mechanism can be predicted using the following equation for air column vibration in open cylinders [4]:

$$f = \frac{Nc}{4(h + 0.3D)} \quad (2)$$

which predicts a frequency that varies inversely with cavity depth.

A schematic diagram of circular cavity geometry is seen in Figure 2. Several differences have been noted between the flow over cavities of circular planform and those of rectangular and elliptical planform. For instance, when comparing their drag for various depth to stream-wise length ratios (h/l) similar drag trends are observed at most depths, but for h/l equal to about 0.5 the circular case has a far greater drag than the rectangular or elliptical cases [5]. Along with the peak in drag noted at this configuration, a strong asymmetry about the stream-wise central axis of the cavity is also seen in the mean pressure distribution along the cavity surfaces [5]. This phenomenon marks a rare instance for which an asymmetric mean pressure distribution is found for a symmetric geometry. Gaudet and Winter [6] later discovered that the flow at most depth configurations (usually stated in terms of the cavity depth to diameter ratio: h/D) consisted of a single large recirculation vortex with axis perpendicular to the stream-wise

centreline of the cavity and rooted to opposite sides of the cavity inner sidewall. However, for the case of $h/D \approx 0.5$ the axis of the recirculation vortex appeared at about 45° to the stream-wise centreline and was only rooted to one point on the upstream cavity sidewall, such that the vortex axis angled upwards and exited the cavity at the downstream edge to form a trailing vortex downstream of the cavity [6]. The investigators reasoned that the peak in the drag noted at this depth was due to the exposed recirculation vortex sweeping more fluid into the cavity. This trailing vortex flow was stable for any given trial and Gaudet and Winter reported that the vortex tended to originate from one particular side of the cavity. However, occasionally the “sense” of the vortex was found switched such that the vortex originated from the opposite side of the cavity, effectively reflecting the usual mean flow pattern across the cavity streamwise centreline. Gaudet and Winter and later investigators Hiwada et. al. [7] also reported that it was possible to switch the sense of this trailing vortex by applying a disturbance to the approach flow of the cavity. Details of this disturbance were not reported, however.

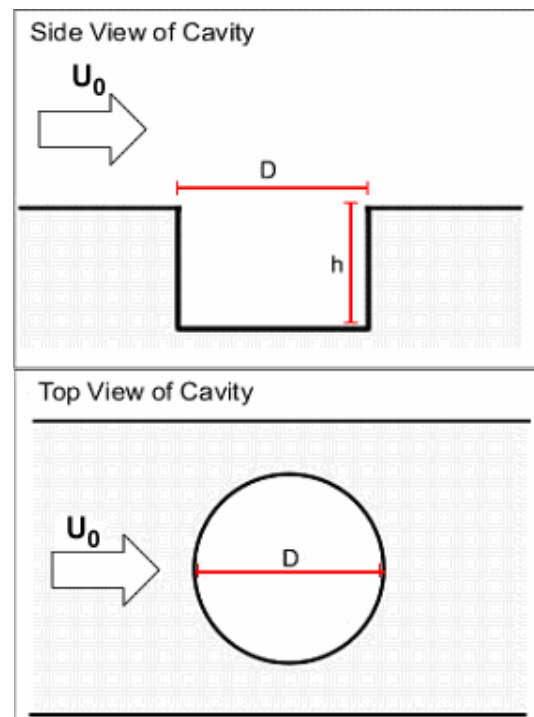


Figure 2: Schematic diagram of circular cavity geometry.

Hiwada et. al. proposed a set of flow regimes based on the h/D ratio of the cavity by observing

mean pressure patterns along the cavity surfaces along with the appearance of the pressure time series at points on the cavity surfaces at these various depth configurations [7]. Pressures for these types of flows are often stated in terms of a pressure coefficient C_p , defined in equation (3) or for fluctuating pressures, $C_{p_{RMS}}$, defined in equation (4). This allows a presentation of the measured pressures in relation to the free stream dynamic pressure.

$$C_p = \frac{p - p_s}{\frac{1}{2} \rho U_0^2} \quad (3)$$

$$C_{p_{RMS}} = \frac{\sqrt{(p - \bar{p})^2}}{\frac{1}{2} \rho U_0^2} \quad (4)$$

Single spanwise lines of mean streamwise velocity [7,8] and turbulence [8] were also reported and these results served as further evidence for asymmetric mean flow for $h/D \approx 0.5$ and symmetric mean flow for other depths.

The present study aimed at finding an explanation for the high drag and mean flow asymmetry noted for $h/D \approx 0.5$ and also aimed to investigate the fluctuating nature of the flows at various depth configurations.

2. EXPERIMENTAL DETAILS

Experiments were carried out in a closed-loop subsonic wind tunnel in the Boundary Layer Wind Tunnel Laboratory at the University of Western Ontario. The tunnel had working section dimensions of 6.50 m length \times 0.61 m width \times 0.21 m height and a free-stream velocity of 27.0 m/s was used for testing. All measurements were conducted with the cavity model centre located at 4.29 m downstream of the working section inlet. The Reynolds' number based on cavity diameter was 1.3×10^5 . Other relevant boundary layer parameters for the experiments are listed in Table 1.

Both the cavity models used for measurements were built of acrylic and had a fixed diameter of 76 mm. The depth of the cavity was adjustable by movement of the piston-like cavity base, although measurements were limited to depths of 0.2, 0.47 and 0.7 D in this study.

Flow Quantity	Value	Range*
δ	55 mm	± 5 mm
δ_*	7.0 mm	± 0.9 mm
δ_θ	5.1 mm	± 0.7 mm
c_f	0.0030	± 0.0001
u_* / U_0	0.042	± 0.0007

*Range refers to the maximum deviation of a series of measured values measured at a variety of spanwise points across the working section from -1.0D to +1.0D. Quantities stated in the "Values" column are the mean values of these spanwise measurements.

Table 1: Approach flow parameters used for experiments.

Figure 3 below shows a schematic diagram of the experimental geometry.

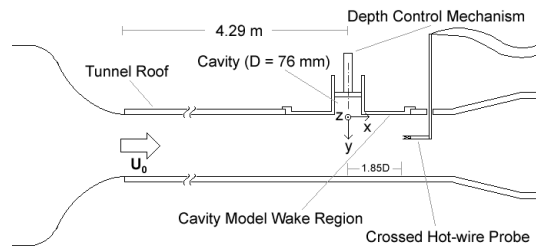


Figure 3: Schematic diagram of experimental geometry (not to scale).

The free-stream velocity was monitored at all times using a Pitot-Static tube positioned slightly downstream of the cavity model and offset spanwise from the cavity centre.

2.1 Surface Pressure Measurements

An acrylic cavity model was fitted with flush-mounted pressure taps to allow the measurement of mean and fluctuating pressures at the cavity surfaces. The pressure taps had an inner diameter of 0.5 mm, and a total of 40 taps were distributed in linear configurations about the cavity surfaces with 10 on the cavity base, a maximum of 12 on the sidewall (depending on the cavity depth), and 16 in the cavity wake region.

These lines of pressure taps were rotated with the cavity model in 10° increments to produce well-

resolved mean pressure contours on the cavity surfaces.

Pressures were measured using Honeywell DCAL4 and NDR4 differential pressure transducers with a range of $\pm 1''$ (25.4 mm) WG and uncertainty of $C_p = \pm 0.003$, which were sampled at 1,000 Hz / channel for 30 s sample lengths using a PC-controlled data acquisition system. This pressure measurement apparatus had a frequency response that was reasonably constant up to approx. 100 Hz after which it attenuated considerably. Hence, only low frequency fluctuations were measured accurately with these devices.

From the pressure-time series at each of the measurement points, the mean and RMS values were calculated and charted in the form of contour plots to analyze the patterns in these quantities across the cavity surfaces. The drag due to the presence of the cavity was also calculated by numerically integrating the downstream component of the mean pressures on the cavity sidewall.

2.2 Acoustic Measurements

A separate cavity model of identical geometry and depth variability as the pressure tapped model was built with a series of 13 holes each of 6 mm diameter to flush-mount Panasonic WM-61B miniature electret microphones along the cavity surfaces. The microphones were distributed along the cavity surfaces with 9 on the cavity base, a maximum of 3 on the sidewall (once again, dependent on the cavity depth setting), and 1 on the cavity wake surface.

These microphones were rotated along with the model at 20° increments in order to record the fluctuating pressure at the model surfaces at a variety of points. Data from the 13 microphones were sampled simultaneously at a rate of 10,000 Hz / channel for 30 s sample lengths, allowing fluctuations from 0 to 5,000 Hz to be resolved. The frequency spectra of the measured pressure data from the microphones was the desired result of these measurements, and since only the fluctuations due to the presence of the cavity were of interest, various filtering techniques were employed to isolate these fluctuations from those due to other sources.

2.3 Wake Velocity Measurements

Velocity measurements were made in the cavity wake by traversing a Dantec 55P61 crossed hot-wire probe through a slot $1.85 D$ (141 mm) downstream of the cavity model centre, as pictured in Figure 4. Uncertainty for the measured streamwise velocity was always less than ± 0.4 m/s.

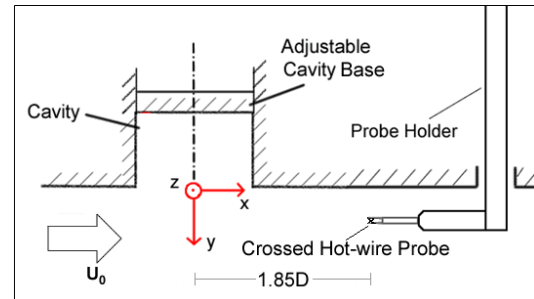


Figure 4: Schematic diagram of hot-wire apparatus setup and cavity-centred coordinates.

A two-axis traverse moved the probe through a rectangular grid of 66 measurement points (6 rows of 11 spanwise points). The spanwise centre of the grid was lined up with the spanwise centre of the cavity and the points ranged from $-D$ to $+D$ in the spanwise direction (z-axis) and from $0.02D$ to $0.415D$ in the vertical direction (y-axis).

The two channels of the hot-wire signal were acquired simultaneously at 20,000 Hz / channel for a sample length of 30 s for each measurement point in the grid. Velocity time series were calculated from the hot-wire output and these were used to find the mean and RMS values for the streamwise velocity, which was the component of greatest interest for this study. To isolate the cavity effect on the wake flow from the background approach flow, the velocity measured with no cavity in place was subtracted from the velocity measured with the cavity model in place.

2.4 Wake Flow Control Experiment

To investigate the ability to switch the sense of the wake flow asymmetry for $h/D \approx 0.5$, as reported by previous investigators [6,7], an experiment was conducted to determine the nature and strength of upstream disturbance required to cause this flow switch to occur. A depth of $h/D = 0.47$ was chosen for this experiment due to a previous report that this was

the depth for which the highest level of drag and flow asymmetry had been observed [6]. A 1.25 cm × 39 cm spanwise slot was cut in the tunnel roof 0.58 m upstream of the cavity model centre allowing the introduction of a 1 cm thick sheet of plywood to the flow. The width of the plywood sheet was 30 cm and, thus, being narrower than the slot, an asymmetric transient blockage disturbance of the boundary layer flow upstream of the cavity was possible. The sense of the flow asymmetry inside the cavity was monitored during this experiment by measuring surface pressures, using the pressure tapped cavity model. As seen in Figure 5, it was established by previous investigators [6,7,8] that a region of low pressure on the cavity sidewall near the downstream lip near $\theta = 240^\circ$ indicated the departure of the recirculating vortex from the cavity into the external flow. On the other side of the cavity near $\theta = 160^\circ$, a high pressure region is observed due to the reattachment of the separated shear layer onto the cavity wall at this point. A switch in the sense of the asymmetric flow effectively reflects the mean pressure distribution about $\theta = 180^\circ$, and thus, it is possible to determine if a flow switch has occurred by monitoring the pressure at these two points on the cavity lip. A switch of the trailing vortex from the right side (210°) to the left side (150°) would be seen in the pressure time series at these two points, going from high to low pressure at $\theta = 150^\circ$ and low to high pressure at $\theta = 210^\circ$. This method was originally employed by Hiwada et. al. [7].

The variables used in the experiment were: the side of the applied asymmetric blockage, the area of exposed board and the duration of board exposure.

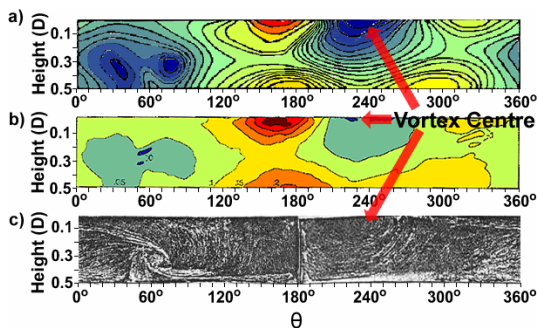


Figure 5: Mean pressure contours along the “unwrapped” cavity sidewall for $h/D = 0.5$, low pressures are blue and high pressures are red, from Hiwada et. al. (a) [7], Savory et. al. (b) [8] and a surface oil-film pattern from Gaudet and Winter [6] showing vortex centre near 240° .

3. RESULTS AND DISCUSSION

Mean and fluctuating surface pressures are presented in this section, along with velocity profiles in the cavity wake region and results from the wake flow control experiment. To establish the accuracy of these results, a graph comparing the resulting incremental drag coefficients ($C_D - c_f$) measured from the present experiment to similar drag measurements from previous investigations is seen in Figure 6. The present results fit the trend from previous results very well.

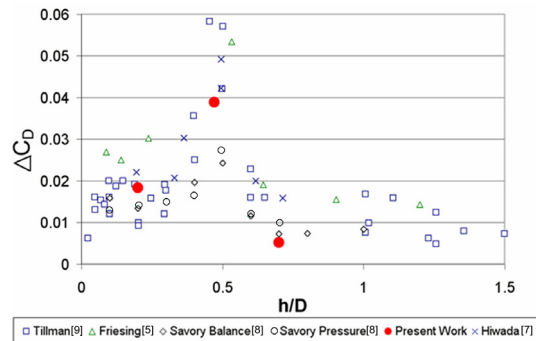


Figure 6: Comparison of incremental drag coefficient results from present experiment to previous results. Results from [9], [5], [8], [8], present, and [7], respective to order in legend.

3.1 Surface Pressure Measurements

Mean pressure patterns on the cavity surfaces for all three depths tested matched well with previous results published by Hiwada et. al. [7] and Savory et. al. [8]. Contours of C_{pRMS} were also generated for each of the cavity surfaces from the same data sets as the mean patterns. Figure 7 shows fluctuating pressure contours for $h/D = 0.20$ and both the sidewall and base images show a remarkable degree of symmetry about the streamwise centreline of the cavity. The intense fluctuation area seen in the sidewall image of Figure 7 centred about $\theta = 180^\circ$ is due to the impingement of the turbulent fluid from the reattachment of the turbulent shear layer on the sidewall at this point. This draws turbulent fluid into the cavity, down the cavity sidewall and drives a reverse flow along the cavity base towards the upstream wall, as evidenced by the high fluctuation levels at the downstream lip with contours perpendicular to the direction of fluid motion.

Figure 8 shows similar images for the $h/D = 0.47$ case, and a clearly asymmetric flow is

demonstrated for this geometry. High fluctuation levels once again mark the shear layer reattachment zone on the downstream cavity sidewall. High fluctuations are also seen on the cavity base at this downstream side, showing the fluid is being drawn down into the cavity at this location. The flow at this configuration is obviously more complex than for the $h/D = 0.20$ case, and this is demonstrated by the nearly circular-shaped fluctuation maxima on the cavity base near the outer rim at $\theta = 35^\circ$ and on the cavity sidewall slightly more than halfway down, centred at $\theta = 70^\circ$. These circular regions are coincident with circular regions of low pressure in the mean pressure +

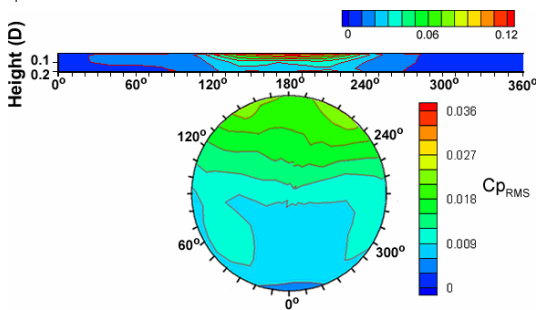


Figure 7: Fluctuating pressure contours (in units of Cp_{RMS}) on cavity sidewall (top) and base (bottom) for $h/D = 0.20$.

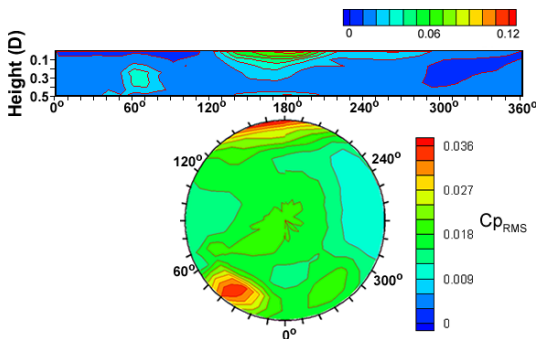


Figure 8: Fluctuating pressure contours on cavity sidewall and base for $h/D = 0.47$.

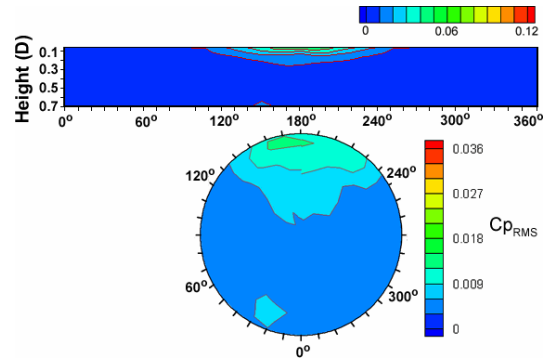


Figure 9: Fluctuating pressure contours on cavity sidewall and base for $h/D = 0.70$.

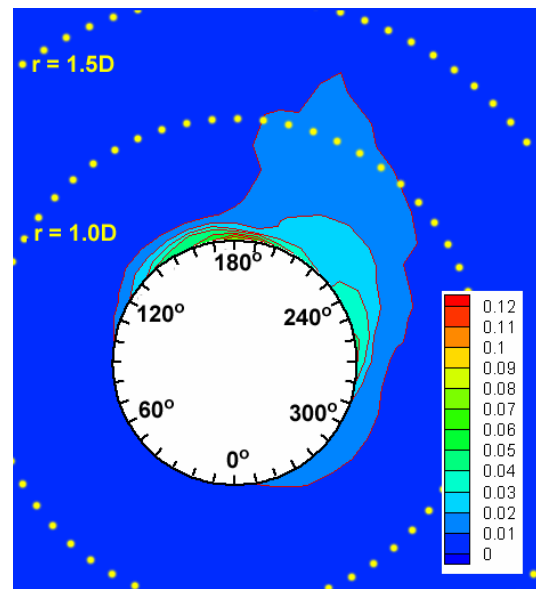


Figure 10: Fluctuating pressure contours (Cp_{RMS}) in cavity wake region (cavity base is cut out) for $h/D = 0.47$, showing asymmetry to right.

distributions, and these regions are also coincident with swirling regions from surface oil-film pictures taken by Gaudet and Winter [6]. This corroborating evidence suggests that these are points where strong vortex structures are rooted to the cavity surfaces. Evidence from the mean pressure contours and oil-film diagrams also suggests that the vortex rooted to the sidewall at $\theta = 70^\circ$ stretches diagonally across the cavity to the downstream lip of the sidewall at $\theta = 235^\circ$ where the vortex leaves the cavity and convects downstream in the external flow as a trailing vortex, noted by the high fluctuation pressure region in the cavity wake zone (Figure 10) near the cavity rim. The interaction between this vortex and the one rooted to the cavity base

is not yet understood due to a lack of information on the flow inside the cavity away from the cavity surfaces.

Figure 9 shows the fluctuating pressure contours for $h/D = 0.70$ and, like the $h/D = 0.20$ case, the distributions are quite symmetric. This geometric configuration shows the lowest pressure fluctuation levels of the three depths tested, suggesting that this case results in the least amount of turbulent external fluid being drawn down into impingement with the cavity surfaces. The less linear nature of the contour lines on the cavity base, paired with more curved contour lines on the cavity base, in the mean pressure distribution suggest a more three-dimensional reversed flow along the cavity base (essentially a radial outflow from the downstream edge of the cavity base).

3.2 Acoustic Measurements

Peaks in the acoustic spectra measured inside the cavity were expected to be driven by the fluid-dynamic and fluid-resonant mechanisms. Using equation (1) and substituting the cavity diameter D for the variable l , oscillations driven by the fluid-dynamic mechanism would be expected at a frequency of 145.5 Hz for a first mode oscillation, whilst equation (2) predicts frequencies of 2,329 Hz for $h/D = 0.20$, 1,512 Hz for $h/D = 0.47$ and 1,164 Hz for $h/D = 0.70$, for the fluid-resonant mechanism.

Power spectral density plots are presented in Figures 11 and 12 for data acquired from various microphones placed along the cavity surfaces for the three cavity depths tested. Spectra have also been calculated for pressure data from the microphones for the no-cavity case ($h/D = 0.00$), and Figures 11 and 12 are actually the result of subtracting the no-cavity spectrum from the cavity-related spectrum at the given measurement point in an attempt to isolate cavity-related oscillations from tunnel-related and ambient noise.

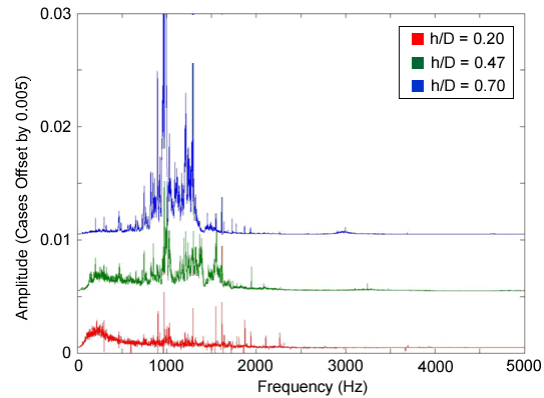


Figure 11: Broadband frequency response of cavities measured with microphone at centre of cavity base.

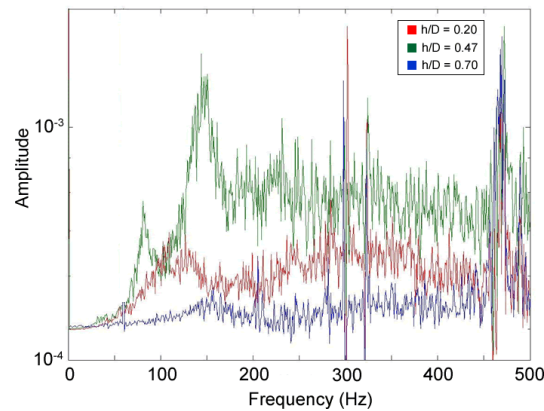


Figure 12: Narrow band frequency response of cavities measured with microphone at centre of cavity base, peak at 147.5 Hz for $h/D = 0.47$ is featured.

The broad spectrum figures (Figure 11) show broadband high frequency acoustic generation, in the range of 700 – 1,500 Hz, for the deeper cavities tested: $h/D = 0.47$ and 0.70 . These broadband features are likely related to cavity geometry: although these broadband features have a similar shape between the $h/D = 0.47$ and 0.70 case, the feature for $h/D = 0.70$ occurs at a lower frequency range, due to the greater cavity depth for this case. The features are possibly related to the fluid-resonant oscillation mechanism due to the fact that they give a high amplitude near the predicted frequencies of 1,512 Hz for $h/D = 0.47$ and 2,329 Hz for $h/D = 0.70$. This evidence is more pronounced for the $h/D = 0.47$ case, where a strong peak is centred at 1,545 Hz. The fact that no such feature is seen in the PSD plot for $h/D = 0.20$ further indicates that the fluid-resonant mechanism may be the

cause of these features, since this type of oscillation is unlikely for shallow cavity depths.

In the lower frequency range (Figure 12), a notable strong peak centred about 147.5 Hz is seen in the PSD plot calculated from the data collected by the microphone in the cavity base for $h/D = 0.47$. This peak is very close to the value of 145.5 Hz predicted for the fluid-dynamic oscillation mechanism, which suggests that this peak was indeed caused by cavity feedback resonance. No other depth tested displays this sharp peak, suggesting that this feedback resonance may be part of the reason for the asymmetric flow and significantly higher drag observed at this configuration and not at other depths.

3.3 Wake Velocity Measurements

Streamwise velocity and turbulence profiles were acquired in the cavity wake for configurations of $h/D = 0.20$ and $h/D = 0.47$. Two profiles were acquired for $h/D = 0.47$, one for each of the stable states for this cavity flow. Once again, an attempt was made to isolate the cavity effect on the flow from the approach flow of the cavity. To do this, similar profiles were measured at the same measurement points with no cavity in place ($h/D = 0.00$) and the mean and turbulent statistics calculated from these data were subtracted from the cases with the cavity in place. The resulting values were normalized by the free stream velocity U_0 to display the cavity effects in terms of the velocity of the approach flow to form the mean velocity unit $\Delta \bar{u}$ and the turbulent quantity Δu_{RMS} . These figures are presented in Figures 13 and 14.

It is clear that the $h/D = 0.47$ case caused the greatest mean streamwise velocity deficit (Figure 13c), reaching a maximum of 11.6% of U_0 for the right-handed profile centred at $z = 0.35D$. The profiles assumed the expected qualitative appearance, with those for $h/D = 0.20$ (Figures 13a and 14a) being quite symmetric about the spanwise centre and the $h/D = 0.47$ cases (Figures 13b,c and 14b,c) being wildly asymmetric. The distributions for the two stable states of the asymmetric flow were nearly mirror images of one another, reflected about the spanwise centreline. Also, the nearly circular features in the plots for $h/D = 0.47$, centred at $z = \pm 0.35 D$ depending on the sense of the flow, are evidence of the presence of the trailing vortex convected from the downstream edge of

the cavity for this configuration. These features are then cross sections of the trailing vortex in this plane. In all cases, regions of high mean streamwise velocity loss are coincident with regions of high streamwise turbulence intensity, showing the conversion of energy from the mean streamwise velocity into turbulent kinetic energy. As expected, for the $h/D = 0.20$ case, the regions of high mean streamwise velocity loss and turbulence intensity are found almost exclusively in the spanwise range of the cavity, from $z = -0.5D$ to $+0.5D$, showing that these wake features are a result of the cavity presence.

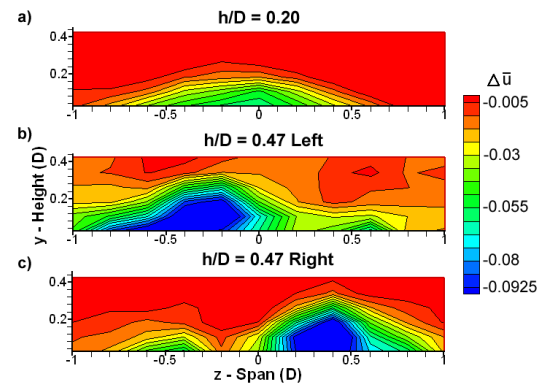


Figure 13: Cavity effect on mean streamwise velocity distribution in wake of cavity model.

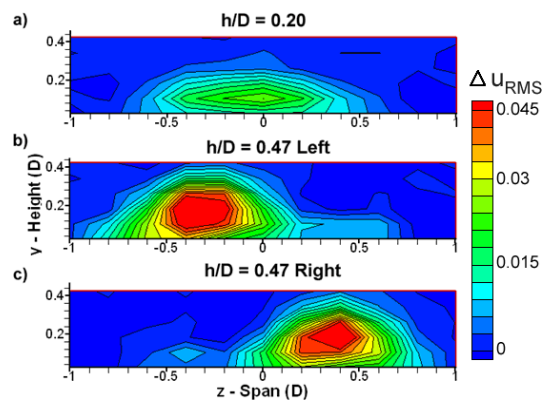


Figure 14: Cavity effect on fluctuating (RMS) streamwise velocity distribution in wake of cavity model.

3.4 Wake Flow Control Experiment

Wake flow switches were monitored using the pressure transducer method described in section 2.4. An example of a pressure-time series generated using this method is seen in Figure 15.

Through the trial of different senses, durations and strengths of upstream disturbance to the approach flow of the cavity for $h/D = 0.47$, it was found that the flow in the cavity and in its wake could be reliably switched by applying a certain strength and duration of disturbance to the flow on the side at which the trailing vortex was observed. For example, if it was observed that the trailing vortex was emerging from the right-hand (+z) side of the cavity, a disturbance with the required strength and duration applied to the right side (+z) of the working section in the approach flow would cause the trailing vortex to switch sides so that it emerged from the left side (-z) of the cavity. A disturbance of the same strength and duration applied to the opposite side, would not cause a successful switch. For the purpose of this discussion, a disturbance applied to the approach flow on the trailing vortex side will be termed a “same-sided” disturbance, while one applied to the side opposite of the trailing vortex will be termed “off-handed”. The pressure-time series in Figure 15 shows the application of an off-handed disturbance at 12 s followed by a same-handed disturbance of the same strength and duration at 26 s. As seen in the trace, the first switch attempt was unsuccessful and the second attempt caused the mean pressure to change from a low value to a high value, indicating that the trailing vortex had moved from the current measurement position to the opposite side.

It was found that the success of a switch attempt was not only dependent on the side of the disturbance, but also on the strength and duration (see Figure 16). A short series of same-handed disturbances were carried out with a variety of exposed plywood board areas and durations, to roughly determine the requirements for a flow switch to take place. The results of these tests are summarized in Table 2 where the × symbol represents a failed flow switch attempt and the ● symbol represents a successful one.

As shown in the table, successful flow switches were made for 1 second disturbances with 36% working section blockage, and for 3 second disturbances with 14.4% blockage and greater. From analyzing the pressure-time series from these tests, there appears to be a link between the induced surface pressure drop at the measurement point and the success or failure of the switch attempt. From this brief investigation the minimum disturbance-induced pressure drop required to cause a flow switch is approximately $C_p = 0.5$. The link between induced pressure

drop and flow switch is further supported by the results in Table 2, in that a greater blockage area is required for the 1 second disturbance than for the 3 second disturbance. A greater exposed blockage area would result in a greater induced pressure drop, as would a greater disturbance duration (until the flow behind the blockage plate reached steady state, after which point increasing the disturbance duration would no longer increase the pressure drop).

Blockage Area		Duration (s)	
In m^2	Working section fraction*	1 s	3 s
0.009	7.2%	×	×
0.018	14.4%	×	●
0.027	21.6%	×	●
0.036	28.8%	×	●
0.045	36.0%	●	●

* This refers to the percentage of the cross-sectional area of the tunnel working section blocked by the exposed plywood board (× = failed switch, ● = successful switch).

Table 2: Results of wake flow switch experiment.

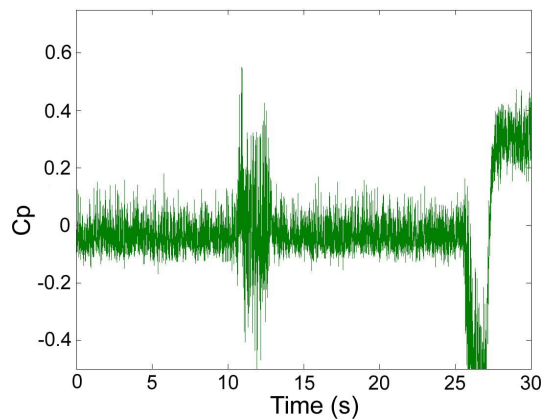


Figure 15: Pressure-time series showing off-handed disturbance (12 s) followed by same-handed disturbance of same strength (26 s).

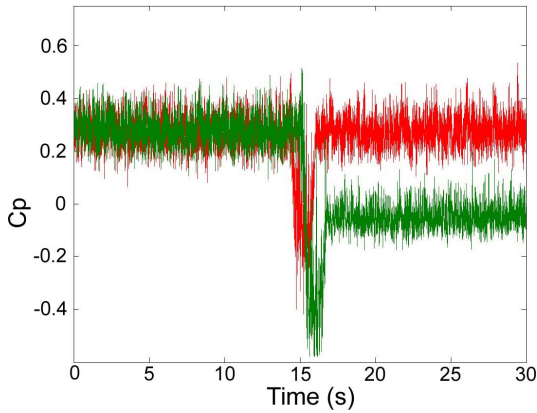


Figure 16: Superposed pressure-time series showing same-handed disturbances of low strength (red) and high strength (green).

4. CONCLUSIONS

The nature of the fluctuating flow field associated with cavities of circular planform has been clarified. Regions of intense surface pressure fluctuation coincide with noted shear layer reattachment zones and wall-rooted vortex centres observed from mean pressure profiles. Low frequency oscillations are measured inside the cavity for the more shallow cavity depths tested ($h/D = 0.20, 0.47$), due to the strong entrainment of external turbulent fluid into the cavity at these configurations. A particularly strong peak noted at 147.5 Hz for the $h/D = 0.47$ configuration is quite likely due to the fluid-dynamic cavity feedback resonance mechanism, and, not being observed at other depths, this oscillation could be a cause of the asymmetric flow and high drag noted at this configuration. In order to improve the support for this explanation, a frequency analysis of the oscillating pressures on the cavity surfaces should be carried out for a greater range of cavity depths from $h/D = 0.1$ to 1.0 to see if only configurations for which $h/D \approx 0.5$ exhibit this strong peak at the frequency predicted for cavity feedback resonance. Broadband high frequency oscillations are noted for the deeper cavities ($h/D = 0.47$ and 0.70) suggesting the presence of an oscillation mechanism that is dependent on cavity depth.

For aerodynamic applications it seems best to keep circular cavities to dimensions of $h/D \leq 0.3$, as cavities fitting this requirement have been noted by previous investigators to have a low drag coefficient and such cavities have been

observed in the present study to produce a great deal less high-frequency acoustic noise than deeper cavities.

Further evidence has been found for the existence of a trailing vortex structure for $h/D = 0.47$ with the appearance of a circular cross-section region of the vortex in the turbulence intensity measured downstream of the cavity model offset from the cavity centre, and a similarly located mean streamwise velocity deficit region has also been measured. A two-dimensional mean velocity field in this plane downstream of the cavity could further support the evidence for this vortex structure.

A reliable mechanism has been found for switching the asymmetric mean flow in the cavity for $h/D \approx 0.5$, which involves the blockage of the boundary layer flow upstream of the cavity on the side which the trailing vortex is observed. Some requirements have also been defined on the strength and duration of the disturbance required to cause this switch.

For applications of the flow switch control mechanism outside of a wind tunnel or duct environment, it may be appropriate to base the blockage parameter on boundary layer thickness or cavity diameter.

5. NOMENCLATURE

c	Local speed of sound
c_f	Local skin friction coefficient
C_p	Pressure coefficient
$C_{p_{RMS}}$	Fluctuating pressure coefficient
D	Cavity diameter
f	Frequency of oscillation
h	Cavity depth
l	Streamwise length of a rectangular cavity
m	Integer mode number
M	Free stream Mach number
N	Odd integer mode number
P	Measured pressure
P_s	Static pressure

PSD	Power Spectral Density
u_*	Friction velocity
U_0	Free stream velocity
x	Streamwise co-ordinate, origin at cavity centre
y	Vertical co-ordinate, origin at cavity lip
z	Spanwise co-ordinate, origin at cavity centre
δ	Boundary layer thickness
δ_*	Displacement thickness
δ_θ	Momentum thickness
ΔC_D	Incremental drag coefficient
$\Delta \bar{u}$	Cavity effect on mean streamwise velocity, normalized by U_0
Δu_{RMS}	Cavity effect on streamwise RMS velocity, normalized by U_0
γ	Vortex impingement / acoustic tone lag factor
κ	Ratio of vortex convection velocity to free stream velocity
θ	Angular co-ordinate, 0° at upstream side of cavity, 180° at downstream side
ρ	Density of air
τ_w	Wall shear stress

6. ACKNOWLEDGEMENTS

This work was financially supported by NSERC. Research assistance was provided by UWO MEng candidates Rita Patel and Tom Hering and additional expertise was provided by the employees at the UWO Machine Shop (UMS), the UWO Engineering Electronics Shop and technicians at the BLWTL at UWO.

7. REFERENCES

- [1] Rossiter, J. E., Wind-Tunnel Experiment on the Flow over Rectangular Cavities at Subsonic and Transonic Speeds, British ARC R&M no. 3428, 1964.
- [2] Ukeiley, L., Murray, N., Velocity and Surface Pressure Measurements in an Open Cavity, Experiments in Fluids, **38**:656-671, 2005.
- [3] McGregor, O. W., White, R. A., Drag of Rectangular Cavities in Supersonic and Transonic Flow Including the Effects of Cavity Resonance, AIAA Journal, **8**:1959-1964, 1970.
- [4] Sen, S.N., Acoustics – Waves and Oscillations, Wiley Eastern Ltd., 1990.
- [5] Friesing, H., Measurement of the drag associated with recessed surfaces: cut-outs of rectangular and elliptical planform. Z.W.B.F.B. 628 (RAE Library Translation 1614, 1971), 1936.
- [6] Gaudet, L., Winter, K.G., Measurements of the drag of some characteristic aircraft excrescences immersed in turbulent boundary layers, RAE Tech Memo Aero 1538 (also AGARD CP124, 1973), 1973.
- [7] Hiwada, M., Kawamura, T., Mabuchi, I., Kumada, M., Some Characteristics of the Flow Pattern and Heat Transfer past a Circular Cylindrical Cavity, Bulletin of the JSME, **26**(220): 1744-1752, 1983.
- [8] Savory, E., Toy, N., Gaudet, L., Effect of lip configuration on the drag of a circular cavity, Emerging Techniques in Drag Reduction, Mechanical Engineering Publications Ltd., 317-335, 1996.
- [9] Tillman, W., Additional measurements of the drag of surface irregularities in turbulent boundary layers, NACA TM 1299 (also in "New resistance measurements with surface irregularities in the turbulent boundary layer.", Forschungshefte fur Schiffstechnik, **2**:81-88, (BSRA Trans No. 322), 1953), 1951.